Manjula, B. N., Glaudemans, C. P. J., Mushinski, E. B., & Potter, M. (1976) *Proc. Natl. Acad. Sci. U.S.A. 73*, 932.
Nisonoff, A., Hopper, J. E., & Spring, S. B. (1975) in *The Antibody Molecule*, Academic Press, New York.
Padlan, E. A., Davies, D. R., Pecht, I., Givol, D., & Wright, C. (1976) *Cold Spring Harbor Symp. Quant. Biol. 41*, 627.
Pecht, I., & Lancet, D. (1977) *Mol. Biol., Biochem. Biophys. 24*, 306.
Pecht, I., Givol, D., & Sela, M. (1972) *J. Mol. Biol. 68*, 241.
Rigler, R., Rabl, C. R., & Jovin, T. M. (1974) *Rev. Sci. Instrum. 45*, 580.
Schechter, I., Ziv, E., & Licht, A. (1976) *Biochemistry 15*, 2785.
Schepers, G., Blatt, Y., Himmelspach, K., & Pecht, I. (1978) *Biochemistry 17*, 2239.
Schiffer, M., Girling, R. L., Ely, K. R., & Edmundson, A. B. (1973) *Biochemistry 12*, 4620.
Schilling, J., Clevinger, B., Davie, J. M., & Hood, L. (1980) *Nature (London) 283*, 35.
Schwarz, G. (1968) *Rev. Mod. Phys. 40*, 206.
Smoluchowski, M. V. (1917) *Z. Phys. Chem., Stoechiom. Verwandtschaftsl. 92*, 129.
Thusius, D. (1977) *Biophys. Chem. 7*, 87.
Vuk-Pavlović, S., Blatt, Y., Glaudemans, C. P. J., Lancet, D., & Pecht, I. (1978) *Biophys. J. 24*, 161.
Weigert, M., Perry, R., Kelley, D., Hunkapiller, T., Schilling, J., & Hood, L. (1980) *Nature (London) 283*, 497.
Zeldis, J. B., Konigsberg, W. H., Richards, F. F., & Rosenstein, R. W. (1979) *Mol. Immunol. 16*, 371.
Zidovetzki, R., Licht, A., & Pecht, I. (1979) *Proc. Natl. Acad. Sci. U.S.A. 76*, 5848.
Zidovetzki, R., Blatt, Y., Glaudemans, C. P. J., Manjula, B. N., & Pecht, I. (1980) *Biochemistry 19*, 2790.
Zidovetzki, R., Licht, A., & Pecht, I. (1981a) *Mol. Immunol. 18*, 491.
Zidovetzki, R., Farver, O., & Pecht, I. (1981b) *Eur. J. Biochem. 114*, 97.

Kinetics of Head–Tail Joining in Bacteriophage T4D Studied by Quasi-elastic Light Scattering: Effects of Temperature, pH, and Ionic Strength†

Julyet Aksiyote-Benbasat and Victor A. Bloomfield*

Appendix: Calculation of the Steric Factors Affecting the Head–Tail Joining Reaction

Donald I. Stimpson, Julyet Aksiyote-Benbasat, and Victor A. Bloomfield

ABSTRACT: We have determined the effects of temperature, pH, and ionic strength on the kinetics of attachment of purified T4D heads and tails, with the aim of understanding some of the mechanistic details of this viral assembly reaction. To produce heads for the reaction, we used an osmotic shock resistant mutant deficient in tails and tail fibers ($10^-/18^-/19^-/34^-/36^-/37^-$); for tails, a $13^-/23^-$ mutant was used. We conjecture that the mutation in gene 13 was necessary to prevent connectors from being attached to both heads and tails, thus blocking their joining. To follow the reaction, we used quasi-elastic light scattering (QLS) [Aksiyote-Benbasat, J., & Bloomfield, V. A. (1975) *J. Mol. Biol. 95*, 335–357], in effect measuring the decrease in average translational diffusion coefficient of the heads as tails are attached. The head and tail concentrations were in the range 6×10^{10} and 1.2×10^{11} particles/mL, respectively, corresponding to about (1 or 2) $\times 10^{-10}$ M. This extreme dilution, which is possible because of the high scattering power of the heads, slows down the very rapid bimolecular reaction to $t_{1/2} \approx 400$ s. We were able to measure the QLS autocorrelation function once every 50 s. Over a temperature range from 10 to 37 °C, the second-order rate constant k increased from 0.79×10^7 M^{-1} s^{-1} to 1.46×10^7 M^{-1} s^{-1}. An Arrhenius plot of ln k vs. $1/T$ was linear, yielding E_a = 4.06 kcal/mol, as expected for a diffusion-controlled reaction, and $\Delta S^* = -12.6$ cal/(mol·deg), corresponding to a steric factor of $^1/_{567}$. This is consistent with our previous estimate based on the deviation from von Smoluchowski's diffusion-controlled reaction theory. The pH dependence of k was measured between pH 5.4 and 8.3. It reached a maximum of 2×10^7 M^{-1} s^{-1} at pH 5.8. The falloff in more acid conditions was due to destabilization of the heads. Over the range 5.8–8.3, the pH dependence was fit well by the ionization of a single group with a pK_a of 6.8, such as an imidazole. The ionic strength dependence was measured by maintaining $[MgCl_2]$ = 0.01 M and varying [KCl] from 0 to 0.20 M. Below 0.02 M KCl, k fell sharply, perhaps due to destabilization of the tails. The rate also decreased above 0.02 M KCl, reaching a plateau above 0.10 M. The decrease in rate constant with increasing ionic strength suggests that the reaction brings together groups of opposite charge.

The assembly of bacterial viruses is of interest in its own right and also serves as a model for the assembly of other subcellular structures that involve protein–protein and protein–nucleic acid interactions. While much has been learned about phage assembly by in vitro complementation experiments with crude or semipurified extracts (Casjens & King, 1975), relatively little work has been done on purified systems, where detailed chemical questions can be investigated. Thus, we understand little about the forces that govern the assembly of bacteriophage and which confer on the structure considerable stability under the stresses that arise during the infection process. It

† From the Department of Biochemistry, University of Minnesota, St. Paul, Minnesota 55108. *Received January 23, 1981.* This work was supported in part by Research Grant GM17855 from the National Institutes of Health.

0006-2960/81/0420-5018$01.25/0

is our aim here to provide such understanding for one crucial joint in bacteriophage T4D, that between head and tail.

Previous work on the disassembly of bacteriophage (To et al., 1969) qualitatively established that no covalent bonds or disulfide bridges were involved in joining the structural parts of phage. Their data also indicate that the head–tail junction, unlike the sheath–baseplate or tail fiber–baseplate attachments, is stable to the action of detergents and therefore may not be hydrophobic in character. More recent work by Smith & Cleary (1975), who used laser-induced single-pulse acoustic transients (i.e., pressure pulses) to disrupt the phage, shows that at the levels of force applied, about 1.3×10^{-4} dyn, one major scission occurs at the junction of head and tail. This force, which corresponds to a bond energy of about 20–30 kcal/mol, is not potent enough to break covalent bonds but in a single hit reaction could break five or six noncovalent bonds.

We have undertaken to study the mechanism of the head–tail joining reaction, $H + T \rightarrow HT$,[1] in bacteriophage T4D by determining the effect of solution conditions upon the kinetics of the reaction. In paper 1 (Aksiyote-Benbasat & Bloomfield, 1975), we demonstrated the ability of quasi-elastic light scattering (QLS) to measure accurately the kinetics of such a reaction, which is accompanied by a change in translational diffusion coefficients between reactants and products, when the reaction rate is slow compared to diffusion. We found that the diffusion coefficient of the heads, $D_H = 3.6 \times 10^{-8}$ cm^2/s, is 14% greater than that for the head–tail particles, the product of the reaction, for which $D_{HT} = 3.14 \times 10^{-8}$ cm^2/s. The second-order reaction, slowed down to a half-time of about 500 s by adjusting the head and tail concentrations to about 5×10^{10} particles/mL (about 8×10^{-11} M), was easily followed by QLS. Under a particular set of conditions—22 °C, pH 7.2, 0.02 M Mg^{2+}, and approximately 0.05 M ionic strength—the bimolecular rate constant was about 1×10^7 L/(mol·s). This, we argued, was consistent with a diffusion-controlled reaction subject to constraints on the relative orientation of the heads and tails and perhaps moderately influenced by pH and ionic conditions.

In the present study, we have used QLS to determine the bimolecular rate constant for head–tail joining under a wide variety of temperature, pH, and ionic conditions. Concentration variation shows that the reaction is indeed second order. The activation energy is consistent with a diffusion-controlled reaction. The reaction involves an ionizable group with a pK of 6.8 and brings together head and tail regions of opposite charge. Magnesium ions seem to be required only for stability of the reactants but do not affect the reaction itself. The Appendix deals with the calculation of the steric factors affecting the reaction.

Materials and Methods

(*a*) *Bacteriophage Methods.* (*i*) *Bacteria and Bacteriophages. Escherichia coli* B was used as the nonpermissive host for infection by T4D amber mutants. The permissive host used for phage growth and titering assays was *E. coli* strain B40 suI. All bacteriophage mutants were derivatives of T4D. The mutants used for producing osmotic shock resistant heads, tail fiberless particles, and tailfibers were described in Table I of paper 1. Tails were prepared from a double mutant in genes 13 and 23, T4D am E609, am B17 (X137), supplied by Dr. W. B. Wood.

(*ii*) *Media and Chemicals.* Bacteria for the preparation of phage stocks, lysates, and extracts were grown in L-broth (10 g of tryptone, 10 g of NaCl, 5 g of yeast, 1 g of glucose per L of distilled water, pH 7.3).

Bacteriophage and bacteriophage parts were suspended in BU/10 buffer (0.039 M Na_2HPO_4, 0.0022 M KH_2PO_4, and 0.007 M NaCl) with 0.02 M $MgSO_4$, 0.1 mM $CaCl_2$, 10 μg of DNase/mL, and 10 μg of lysozyme/mL. RNase was added as indicated in the text, and the buffer was adjusted to pH 7.2. Putrescine dihydrochloride was obtained from Sigma Chemical Co. Protease-free ribonuclease A was purchased from the Calbiochem-Behring Corp. and purified precrystalline deoxyribonuclease (DP) from Worthington. All other media were prepared as in paper 1 and filtered consecutively through 0.22- and 0.025-μm Millipore filters to minimize dust contamination. All labware was rinsed with the appropriate filtered buffer before use.

(*iii*) *Preparation of Extracts of Phage-Infected Cells, Phage Stocks, and Phage Parts.* (1) Extracts of phage-infected cells and phage stocks were prepared as described in paper 1 at 30 °C with superinfection at 13 min.

(2) Heads were prepared as described in paper 1 with the following modifications. The extracts were resuspended in a 5-fold volume of BU/10 buffer supplemented with 20 μg/mL DNase and 20 mM $MgSO_4$. Heads pelleted during the fast centrifugations were resuspended with gentle rocking at 4 °C in BU/10 with 20 mM $MgSO_4$ and 0.1 mM $CaCl_2$, pH 7.2 (standard reaction buffer, SRB); 20 μg/mL DNase was added only during the first cycle of low- and high-speed centrifugation.

(3) Tails were prepared by restrictively propagating the double mutant $13^-/23^-$. This mutant, even during prolonged incubation in extracts at 37 °C, does not grow an extension to the tail which inhibits the head–tail assembly process (Coombs & Eiserling, 1977). This precaution was taken because of the more extensive purification of tails necessary to satisfy the requirements of our more sensitive light-scattering apparatus (see Materials and Methods, part b). The extracts were resuspended in 2% the original volume of BU/10 + 5 mM $MgSO_4$, 0.1 mM $CaCl_2$, and 60 mM KCl (BU tails) with 40 μg/mL DNase and lysed with a few drops of chloroform. The preparation was incubated at 30 °C for 20 min before being dispersed by vigorous pipetting. Cell debris, contaminating phage, and particles were discarded by centrifugation at 12000*g* (at tube bottom) for 15 min at 4 °C. EDTA was added to a final concentration of 20 mM. 110 Kunitz units/mL RNase (Kunitz, 1950), which had been pretreated by heating to 90 °C for 3 min and stored frozen, was added and the mixture incubated at 37 °C for 40 min to degrade the ribosomes. The suspension was cleared by centrifugation at 1000*g* for 15 min at 4 °C, and the tails were pelleted at 140000*g*. For minimization of the concentration of undegraded ribosomes cosedimenting with tails, the centrifugation time was recalculated for each preparation as described in paper 1. The tail pellet was resuspended gently in 1 volume of BU tails. RNase treatment was repeated, and the tails were resuspended in BU/10 + 20 mM $MgSO_4$ + 0.1 mM $CaCl_2$ before being washed twice by centrifugation at 140000*g* and resuspended in half-volume. The complementation activity with purified heads was checked be electron microscopy after each step. The UV spectrum was used to monitor the efficiency of the ribosome degradation. Typically the first RNase

[1] Abbreviations used: QLS, quasi-elastic light scattering; T, tails; H, heads; HT, head–tail particles, product of the assembly of purified heads and tails [tail fiberless particles in Aksiyote-Benbasat & Bloomfield (1975)]; *E. coli*, *Escherichia coli* bacterium; SRB, standard reaction buffer (BU/10 buffer + 20 mM $MgSO_4$ + 0.1 mM $CaCl_2$, pH 7.2); EDTA, ethylenediaminetetraacetic acid.

treatment removed up to 95% of the ribosomes. The UV spectrum still peaked around 260 nm, and quasi-elastic light scattering yielded diffusion coefficients higher than expected for tails. After the second RNase treatment, the UV spectrum peaked at 278 nm, with a structure typical for proteins. Ribosome contamination amounted to less than 1% of the tail concentration, and QLS data were indicative of tails alone.

(*iv*) *Concentration Determinations.* (*1*) *Phage and Heads.* The procedure was described in paper 1. In addition, total scattering intensity was monitored to recheck the final dilution of heads in reaction mixtures of heads and tails.

(*2*) *Tails.* The extinction coefficient of tails was estimated to a first approximation to be $\epsilon_{278}^{1\%} = 12.3$ by using the extinction coefficient for P18 (Tschopp et al., 1979) and for core–baseplate complexes (Arisaka et al., 1979) and by correcting for scattering. Concurrently 2 μL of a mixture of heads of known concentration and tails at a series of dilutions was spread on an electron microscope grid, stained with 2% uranyl acetate, and counted to estimate the tail concentration. The UV absorption of each tail sample was determined and used in conjunction with the EM concentration to calculate an extinction coefficient for tails, $\epsilon_{278}^{\text{part/mL}} = 3.5 \times 10^{-14}$ cm^2/molecule, which was within 5% of the above calculated value for a tail molecular weight of 18.2×10^6 daltons (Aksiyote-Benbasat, 1974) for all samples judged of adequate quality for light-scattering experiments (i.e., not requiring a concentration correction for ribosomes). Both methods were used for each sample.

(*b*) *Quasi-elastic Light Scattering.* (*i*) *Light-Scattering Spectrometer.* Since the publication of paper 1, our light-scattering spectrometer has been considerably upgraded. It is of standard design and has recently been described in detail (Bloomfield & Lim, 1978; Wei & Bloomfield, 1980; Pletcher et al., 1980; G. J. Wei and V. A. Bloomfield, unpublished results).

We use a Lexel Model 95 argon ion laser operating at 5145 Å. The beam is focused by a lens on the center of an index matching fluid vat filled with amyl acetate which is circulated for temperature control. The scattered light passes through pinholes and is focused on the aperture of an ITT FW130 photo-counting photomultiplier tube. The signal is amplified by a Products for Research FW130/559 assembly including a preamplifier, an amplifier, and a pulse-height discriminator. A Canberra 1480 pulse-counting linear ratemeter measures the total scattering intensity and is connected to a chart recorder. The signal from the discriminator is also analyzed by a Langley-Ford 64 channel digital correlator which feeds the data into a PDP-8F minicomputer for storage and cumulant analysis (Koppel, 1972). The final data are printed out on a Decwriter and can be stored on diskettes or plotted out in various combinations on an X-Y plotter. The data printed out include the scattering angle, total intensity, z-average diffusion coefficient, $\bar{D}_z$, hydrodynamic radius, and quality factor, or reduced second cumulant $\langle(\delta D)^2\rangle_z/\langle D\rangle_z^2$, which gives the relative variance of D. As the sensitivity of our spectrometer increased, we also had to upgrade our purification procedures, especially for tails. Impurities in the form of ribosomes, which previously were beyond the detection limit of our apparatus, can now contribute up to 5% error to $\bar{D}_z$. This is clearly unacceptable since we are trying to follow a reaction leading to a total decrease in $\bar{D}_z$ on the order of 10%.

(*ii*) *Preparation of Samples for QLS and the Controls.* All heads were prepared at the pH, ionic strength, or magnesium ion concentration, [Mg^{2+}], at which the reaction was to proceed. All tails were prepared in BU/10 + 20 mM $MgSO_4$ + 0.1 mM $CaCl_2$ buffer at high concentration, diluted into the reaction buffer by a factor of at least 10, and then mixed with the heads for reaction. Dialysis was tried as a more conventional approach to preequilibration of heads and tails in the required buffers. The heads proved unstable to long-term dialysis, and the tails had a tendency to unpredictably stick to the membranes.

Reversibility controls were run for each set of experiments by equilibrating heads and tails in the extreme reaction buffers. Heads were then sedimented out of solution, washed, gently resuspended in standard reaction buffer, SRB, and reacted with tails prepared in the same buffer. Tails were checked by equilibration in the specific reactions buffer and dilution into SRB for reaction with heads prepared in SRB. The results were compared to the kinetics achieved by mixing heads and tails prepared and equilibrated in SRB.

The physical stability of heads in specific buffers was checked by monitoring total light-scattering intensity of a preparation of heads diluted into the buffer for a 10–20-min period. A decline in intensity indicates loss of DNA. Concurrently the viscosity, η, of the solution increases due to the presence of free DNA. This lowers the apparent diffusion coefficient, D, according to

$$D = k_B T/6\pi\eta R \qquad (1)$$

where k_B is the Boltzmann constant, T the temperature in K, and R the radius of the particles. During head–tail assembly, $\bar{D}_z$ also decreases from 3.6×10^{-8} cm^2 s^{-1} for heads to 3.14×10^{-8} cm^2 s^{-1} for head–tail particles at 20 °C. Therefore, during each reaction, the light-scattering intensity was closely monitored to ensure that we were following the assembly and not an ejection process.

(*iii*) *Data Collection.* Precision bore glass sample cells were washed in ethanolic HCl and rinsed extensively with distilled deionized water and with double-filtered buffer. For minimization of the number of necessary but cumbersome concentration determinations, the samples were not filtered before use. Instead, the preparation was handled in double-filtered buffers in thoroughly rinsed labware starting with the extract preparation stage.

Each experiment was run in four stages: (a) the head preparation and tail preparation were analyzed to determine their total scattering intensity and the diffusion coefficient of the particles; (b) the buffer was checked for background scattering; (c) heads were diluted into the buffer and analyzed; (d) tails were added to follow the reaction with data accumulated for 50 s/kinetic time point and stored on diskettes. The cycle was repeated every 53.25 s. The first stage is a control on the quality of the heads and the tails and on the purity of the samples. The buffer in which the reaction is run contributes no more than 0.1% to total scattering intensity. The control after the heads are diluted into the buffer tests the accuracy of dilution by checking total intensity; the constancy of the diffusion coefficient confirms that the heads are still intact after dilution into the reaction buffer, and a time-course study on the intensity and diffusion coefficient helps to detect any effect the mixing process might have on the reaction data. Addition of the tails begins the reaction, which is followed to about 80% completion. A final data point is taken at the end of 2–3 h to determine the actual end point of the reaction. In other aspects data collection was as described in paper 1.

(*iv*) *Data Analysis.* Data analysis is done on a PDP-8F minicomputer. The cumulant analysis inherently leads to a correlation between the quality factor and the calculated $\bar{D}_z$ (Wei & Bloomfield, 1980; G. J. Wei and V. A. Bloomfield,

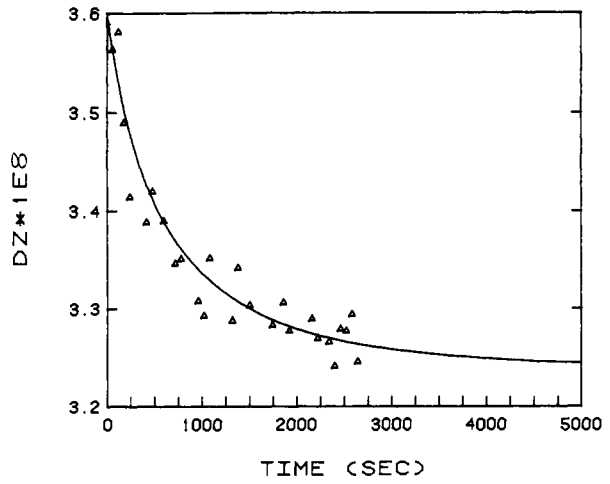

FIGURE 1: Typical plot of $\bar{D}_z$ as a function of reaction time t after correction for linear correlation with quality factor. [H] = 7.15 × 10^{10}/mL and [T] = 1.27 × 10^{11}/mL at 10 °C. The line is calculated from eq 2–4, with k = 7.9 × 10^6 M^{-1} s^{-1}.

unpublished results). Therefore all data were corrected to extract the independent $\bar{D}_z$, carrying only a random error term.

The head–tail association reactions were run under conditions where the zero time tail concentration, $[T]_0$, is slightly greater than the initial head concentration, $[H]_0$, to ensure full conversion of heads to tail fiberless particles.

For a second-order reaction, we then expect

$$kt = \frac{1}{[T]_0 - [H]_0} \ln \frac{[H]_0([T]_0 - [HT])}{[T]_0([H]_0 - [HT])} \quad (2)$$

where k is the second-order rate constant, t is the reaction time, and [HT] is the concentration of tail fiberless particles formed by the reaction. The only unknown in the equation, [HT], has to be determined from $\bar{D}_z$ by remembering that

$$\bar{D}_z = \frac{\sum_i M_i^2 n_i D_i}{\sum_i M_i^2 n_i} \quad (3)$$

where i is the H or HT, the molecular weights are M_H = 176 × 10^6 and M_{HT} = 196 × 10^6, n_i is the molar concentration, and the apparent diffusion coefficients are D_H = 3.6 × 10^{-8} cm^2/s and D_{HT} = 3.24 × 10^{-8} cm^2/s when measured at scattering angle 120° (Wilson & Bloomfield, 1979).

We can neglect the contribution of tails to the scattering because their molecular weight is only 10% of the heads, and they therefore scatter only 1% as much as either heads or tail fiberless particles at equivalent molar concentrations (see paper 1).

Solving eq 3 for [HT], we get

$$[HT] = \frac{[H]_0}{1 + (M_{HT}/M_H)^2[(D_{HT} - \bar{D}_z)/(\bar{D}_z - D_H)]} \quad (4)$$

Then we linearly plot the logarithmic term in eq 2 vs. t. The slope equals $k([T]_0 - [H]_0)$, and the line should run through the origin. Typical data are shown in Figures 1 and 2.

Results

The kinetics of the joining of T4D heads and tails under various solution conditions were followed by mixing the purified parts in the light-scattering cell and following the temporal change in the z-average diffusion coefficient.

(*a*) *Concentration Dependence.* To confirm the second-order nature of the head–tail assembly reaction, we ran a set of experiments with the tail concentration fixed at 4 × 10^{11} particles/mL and varied the head concentration from 3 × 10^{10} to 3 × 10^{11} heads/mL in SRB. The results in Figure 3 show a good correlation between observed and expected reaction half-lives.

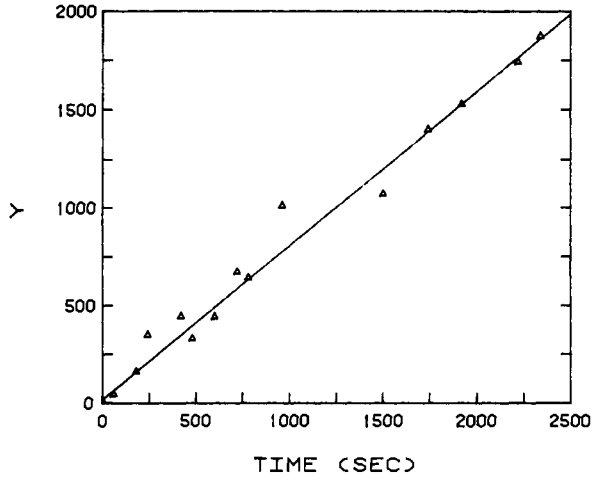

FIGURE 2: Second-order plot of Y = right-hand side of eq 2 vs. t to obtain rate constant k. Conditions are as in Figure 1.

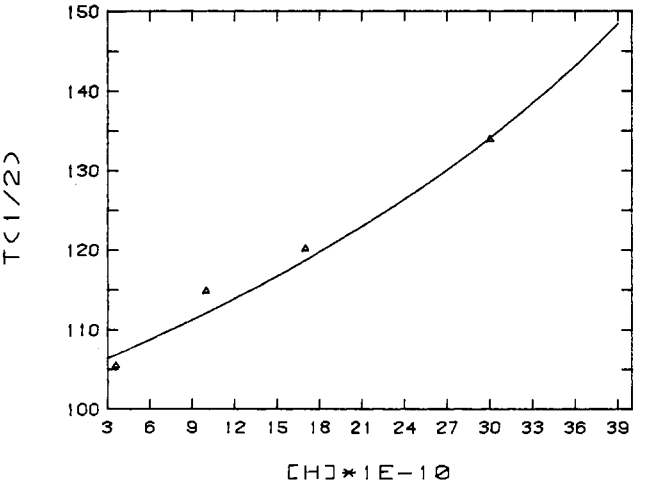

FIGURE 3: Half-life of head–tail joining reaction as a function of head concentration. The line is the expected dependence for a second-order reaction.

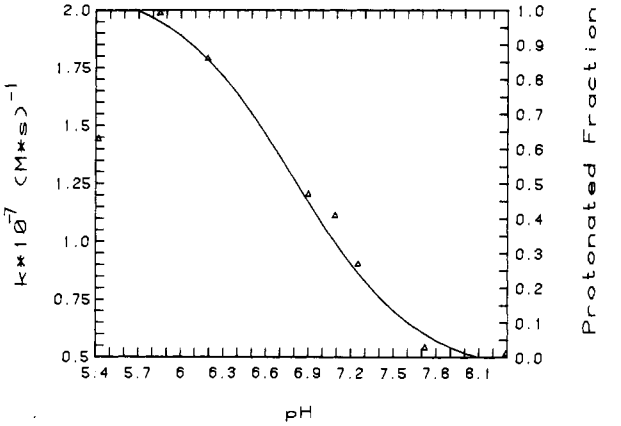

FIGURE 4: pH dependence of second-order rate constant at 30 °C and 0.1 M ionic strength. The solid line is a titration curve for a group with a pK_a of 6.8.

(*b*) *pH Dependence.* pH dependence studies were performed at 30 °C in BU/10 buffer at an ionic strength of 0.1 M. As shown in Figure 4, the rate constant decreases from 2 × 10^7 to 0.5 × 10^7 M^{-1} s^{-1} over the pH range 5.8–7.5 and levels off between pH 7.5 and 8.3. There is a drop in the rate constant at pH's below 5.8. Reversibility controls in SRB for the pH

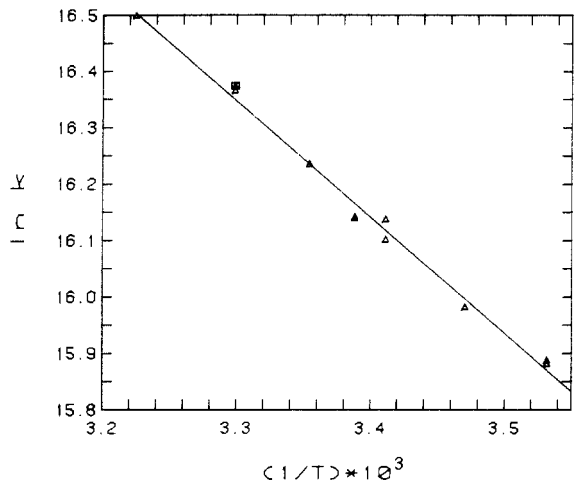

FIGURE 5: Arrhenius plot of rate constant–temperature data in BU/10 buffer at pH 6.9, I = 0.1 M. (△) Data from this study; (▲) paper 1, QLS data; (□) paper 1, complementation data. The solid line is a linear least-squares fit to the data.

extremes show heads to irreversibly lose activity below pH 5.8 but to be fully reactivable after incubation at pH 5.8.

There is a decrease in expected total light-scattering intensity and in diffusion coefficient when heads are diluted into buffer at pH 5.4. Treatment with DNase restores the diffusion coefficient but not the total intensity. This implies that the heads are leaking DNA. Tails are stable at both pH limits.

(*c*) *Temperature Dependence.* Temperature-dependence studies were carried out at pH 6.9 and an ionic strength of 0.1 M between 10 and 37 °C. The data, summarized in an Arrhenius plot in Figure 5, show a gentle increase in rate constant from $\sim 8 \times 10^6$ to 1.5×10^7 M^{-1} s^{-1} over that range.

As indicated by the Arrhenius equation

$$\ln k = \ln s - E_a/RT \tag{5}$$

the slope gives the activation energy of the reaction, E_a = 4060 ± 120 cal/mol. The Arrhenius factor, $s = e^{23.07}$, is determined from the intercept of the plot.

By use of the absolute rate theory (Glasstone et al., 1941)

$$k = \frac{k_B T \kappa}{h} e^{\Delta S^*/R} e^{-\Delta H^*/RT} \tag{6}$$

we relate the activation entropy, ΔS^*, for the reaction to the Arrhenius factor

$$s = e \frac{k_B T \kappa}{h} e^{\Delta S^*/R} \tag{7}$$

where κ is the transmission coefficient, taken equal to unity, and h is Planck's constant. This enables an estimate of the factor $p = \exp(\Delta S^*/R)$ by which the reaction rate is slowed down, relative to the diffusion-controlled limit, by orientational and electrostatic factors (see Discussion). At 20 °C, ΔS^* = −12.6 cal mol^{-1} deg^{-1}, so $p = {}^1/_{567}$.

Both heads and tails are stable between 10 and 37 °C. However, the stability of heads sharply declines at higher temperatures, as indicated by the decrease in both scattering intensity and D and the rise of D after DNase treatment.

(*d*) *Ionic Strength Dependence.* Ionic strength dependence studies, shown by the points in Figure 6, were performed in BU/10 buffer supplemented with 10 mM $MgCl_2$, 0.1 mM $CaCl_2$, and varying concentrations of KCl at pH 7.2. The rate constant decreases steadily from 1.3×10^7 to 0.47×10^7 M^{-1} s^{-1} with increasing ionic strength between 0.05 and 0.23 M. There is also a decrease at ionic strengths below 0.05 M which can be explained by the instability of tails at low ionic strengths. The heads are stable at both limits.

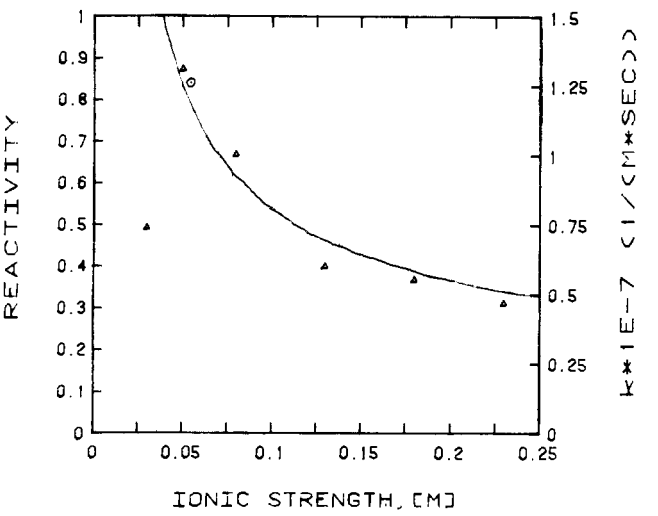

FIGURE 6: Ionic strength dependence of rate constant in BU/10 buffer with 10 mM $MgCl_2$ and 0.1 mM $CaCl_2$ at pH 7.2, 30 °C. The ionic strength was varied by changing [KCl]. (△) Data from this study; (⊙) paper 1, 30 °C, complementation assay. The solid line is the electrostatic effect calculated by using eq 11–13 with $z_1 z_2 = -60$.

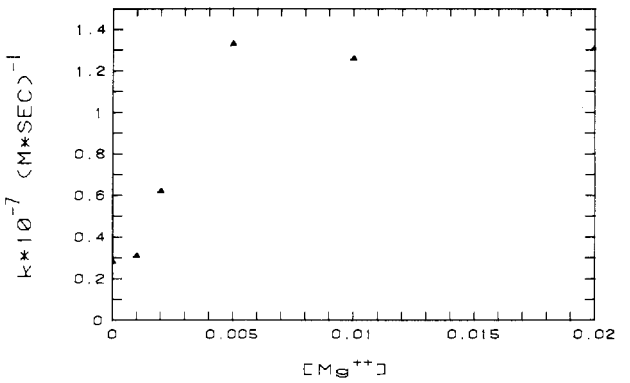

FIGURE 7: Dependence of rate constant on $[Mg^{2+}]$ in BU/10 buffer with 20 mM [$MgCl_2$ + putrescine $(HCl)_2$] and 0.1 mM $CaCl_2$ at 30 °C, pH 6.9.

(*e*) *Mg^{2+} Concentration Dependence.* We studied the dependence of the rate constant on magnesium ion concentration at 30 °C and pH 6.9. The ionic strength was kept constant at 0.08 M (20 mM $MgCl_2$) by replacing $MgCl_2$ with putrescine $(HCl)_2$ which is known to stabilize heads (Harrison et al., 1973). Spermidine was not used in this case because lower concentrations of spermidine are known to cause condensation of DNA (Wilson & Bloomfield, 1979) while Mg^{2+} and putrescine do not. Both heads and tails were stable at concentrations of Mg^{2+} as low as 2 mM. Below that value, heads slowly leaked their DNA while on EM examination tails seemed normal. The rate constant increased with increasing Mg^{2+} concentration and remained constant at $[Mg^{2+}]$ between 5 and 20 mM (Figure 7).

The kinetic measurements reported here agree with, but considerably extend, those reported in paper 1. In the earlier work, performing the reaction in a buffer containing BU/10, 20 mM $MgSO_4$, 0.1 mM $CaCl_2$, and 1 mM spermidine at pH 7.2, we found $k = 1.02 \times 10^7$ M^{-1} s^{-1} at 22 °C using QLS, and $k = 1.28 \times 10^7$ M^{-1} s^{-1} at 30 °C using an infectivity assay. These data are included in Figures 5 and 6.

Discussion

This study illustrates that QLS has considerable advantages in the measurement of kinetics of such assembly reactions, in addition to the obvious ones of rapidity and accuracy, over the conventional infectivity assays of completely assembled phage.

With the latter, the kinetics of the step of interest must be deduced from the cumulative behavior of all assembly steps including and following that one in the reaction pathway. After the head–tail joining reaction, addition of the collar (Coombs & Eiserling, 1977) and the tail fibers to the head–tail particle are required to form an infectious phage. Each of these steps may well have different temperature, pH, and ionic requirements, thereby obscuring the effects of these variables on the reaction of interest.

The pH dependence of the head–tail joining rate shows a bell-shaped curve with a peak around pH 6. The drop in activity at lower pH is due to instability of the heads, while the decrease at higher pH reflects a dependence on the state of protonation of one of the reactants. The data can be fitted to the titration curve of a group (or a set of independent, identical groups) with a pK_a of 6.8, which is active in the protonated form. The fit is shown by the solid line in Figure 4.

Analysis of the temperature dependence of the reaction indicates a low activation energy, about 4 kcal/mol, consistent with a diffusion-controlled reaction. Yet the reaction rate is about 600-fold lower than would be estimated for a diffusion-controlled reaction between two spherically symmetrical reactants by the Smoluchowski (1917) equation

$$k = (4\pi N_0/1000)(D_H + D_T)(R_H + R_T) \qquad (8)$$

With the values $D_H = 3.6 \times 10^{-8}$ cm^2/s, $D_T = 6.0 \times 10^{-8}$ cm^2/s (J. Aksiyote-Benbasat and V. A. Bloomfield, unpublished results), and the center-to-center distance $R_H + R_T$ at reaction estimated from the radius of the head and half the length of the tail as 950×10^{-8} cm, this equation gives $k = 8.2 \times 10^9$ M^{-1} s^{-1} at 20 °C, about 675 times the observed value. This is in reasonable agreement with the factor $p = \exp(\Delta S^*/R) = {}^1/_{567}$ estimated from the Arrhenius plot.

We attribute this reduction in rate constant to steric constraints, which were discussed qualitatively in paper 1. There we noted that only one of the 12 head vertexes is reactive, likewise only one of the two ends of the tail, and that the long axes of head and tail must be nearly collinear for reaction to occur. Matching of the 5-fold symmetry of the head with the 6-fold symmetry of the tail (Moody, 1965; Müller-Salamin et al., 1977) may require additional alignment. In the Appendix we attempt a more quantitative treatment of these effects. We calculate the area of the reactive patches on heads and tails that would allow the joining reaction to proceed at the measured rate, by modifying eq 8 to include rate-enhancing electrostatic and rotational diffusion effects and retarding geometric constraints. The calculated area is 2.4×10^4 Å^2, while the area of the tail tip, taken as a circle of radius 85 Å, is 2.3×10^4 Å^2. The close agreement, though perhaps fortuitous, is gratifying.

Though both heads and tails are negatively charged overall, they behave like reactants of opposite charge in the joining reaction (Figure 6). As the ionic strength increases, the Coulombic attraction between the reactive sites is more shielded by the intervening ion atmosphere, thereby lowering the rate.

A proper treatment of ionic strength effects on this geometrically complicated end-on reaction between a roughly spherical head and a roughly cylindrical tail is not available. Instead, we use a simple point-charge approximation (Debye, 1942), according to which the diffusion-controlled rate constant calculated according to eq 8 is multiplied by a factor

$$f = \left[a \int_a^\infty \exp(\psi/k_B T) dr/r^2\right]^{-1} \qquad (9)$$

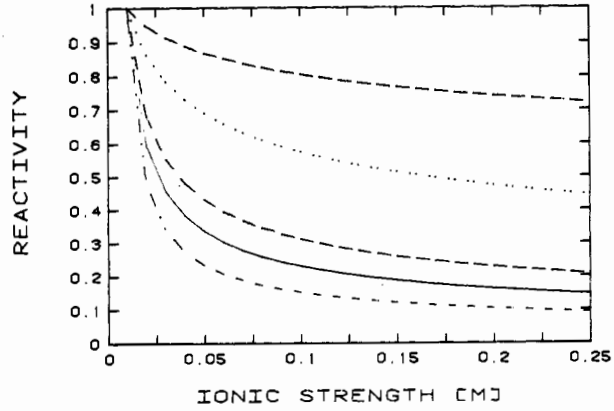

FIGURE 8: Electrostatic effect on the rate constant with the relative rate constant f calculated as a function of ionic strength for various charge products z_1z_2 according to eq 11–13.

where a is the distance of closest approach. We assume a screened Debye–Hückel potential energy

$$\psi = (z_1z_2e^2/\epsilon) \exp(-\kappa r)/r \qquad (10)$$

where the z_i's are the charges on the reactants in units of the electron charge e, ϵ is the dielectric constant of the solution, and r is the distance of separation. κ is the reciprocal thickness of the ion atmosphere, related to the ionic strength I by

$$\kappa = \left(\frac{8\pi N_0 e^2}{1000\epsilon k_B T}\right)^{1/2} I^{1/2} \qquad (11)$$

Figure 8 shows a plot of f calculated as a function of ionic strength for a series of charge products z_1z_2. The curves for low charge products are distinct, while for reactions between highly charged molecules the curves are poorly resolved. In Figure 6 the data are superimposed on the theoretical curve for $z_1z_2 = -60$. Agreement is good, but the poor resolution in this range and the many approximations employed in these calculations preclude any firm assertion other than that the reaction involves relatively highly charged reactants. Charges of 5 or 10 for the head vertex and 6 or 12 for the tail tip would be consistent with the symmetries of these structures (Moody, 1965).

Protein compositions and isoelectric points for some of the head and tail proteins have been determined. The major structural proteins of the head, gp23*, gp22, and gp24, are negatively charged, while the internal proteins are uncharged or slightly positive (Tsugita et al., 1975). The DNA phosphate charges are incompletely neutralized by internal cations, so the head as a whole is highly negative.

The tail, too, is negatively charged as a whole. The amino acid composition of gp18 (Tschopp et al., 1979) points to a negatively charged sheath unless more than 50% of the Asp and Glu residues are in the amino form. Cores and baseplates have pI's in the range 5.1–5.7 (Cummings et al., 1970) and therefore are negatively charged at neutral or higher pH. The gradual dip in the joining rate below pH 5.9 might be due to a charge reversal effect augmented by the inactivation of heads.

The net charge of heads and tails thus predicts that the rate should increase substantially as the ionic strength is raised rather than decrease as observed. This suggests that some positively charged proteins are attached to the head vertex or tail tip and locally outweigh the net negative charge. It further suggests that the local number of positive charges may be greater than the 5–12 suggested above, so as to outweigh the negative charges. It is not known which proteins contribute this negative charge. According to Coombs & Eiserling

(1977), gp13, N2, and/or N6 is located at the head vertex. gpWac, or N1, forms the collar and whiskers but may not be assembled and attached until the head and tail are joined. gp20 has been implicated as the protein imparting 5-fold symmetry to one of the head vertices, while the other 11 contain gp24 (Müller-Salamin et al., 1977). The tip of the tail carries gp14 and gp15 (Coombs & Eiserling, 1977). Unfortunately, none of these protein charges is known.

The effect of Mg^{2+} on the joining reaction seems to be related only to the instability of heads at very low concentrations of magnesium. Tails are not affected at low $[Mg^{2+}]$ so long as the total ionic strength is kept above 4 mM (Arisaka et al., 1979).

When we first planned these experiments, it seemed that the total scattering intensity might be a better indicator than the average diffusion coefficient of reaction progress. According to standard scattering theory, the intensity of scattering from a solution component is proportional to the product of four factors: molecular weight M, weight concentration c, refractive index increment dn/dc, and scattering form factor P. With the assumption that dn/dc is approximately the same for heads and tails and noting that $c = Mn$, where n is the molar concentration

$$\frac{I_{H+T}}{I_{HT}} = \frac{M_H^2 n_H P_H + M_T^2 n_T P_T}{(M_H + M_T)^2 n_H P_{HT} + M_T^2 (n_T - n_H) P_T} \quad (12)$$

Since the head is the major scatterer, we initially assumed that $P_H = P_{HT}$. This leads, with tails in roughly 2-fold molar excess over heads, to $I_{H+T}/I_{HT} = 0.82$. Since $D_{HT}/D_H = 0.87$, we anticipated that the total intensity change would be a more sensitive kinetic probe. However, no increase in intensity could be detected experimentally, while the average D decreased as expected.

The assumption of equal form factors appears responsible for this discrepancy. The general equation, assuming Rayleigh–Debye scattering, is (Geiduschek & Holtzer, 1958)

$$P(q) = \frac{1}{N^2} \sum_{i=1}^{N} \sum_{j=1}^{N} \frac{\sin qr_{ij}}{qr_{ij}} \quad (13)$$

where q is the magnitude of the scattering vector (eq 1, paper 1), r_{ij} is the distance between the ith and jth scattering elements, and N is the number of such elements. This equation must be evaluated numerically for molecules of complex shape. We assumed an assembly of 81 identical spherical elements, 73 in the head, 5 in the tail, and 3 in the baseplate, each 100 Å in radius. This model was used previously for QLS calculations (Wilson & Bloomfield, 1979). The sum in eq 13 was computed from the coordinates of the elements, for head–tail particles and for heads alone. The results gave $P_{HT}/P_H = 0.83$, with a slight dependence on the scattering angle, in gratifying agreement with the ratio $P_{HT}/P_H = 0.81$ required to make the ratio of intensities in eq 14 equal unity.

Thus QLS has advantages over conventional light scattering for studying assembly of large particles that might not have been immediately obvious. It measures change in hydrodynamic size directly, without need to take into account the intraparticle interference effects arising when the scattering particles have dimensions comparable to the wavelength of light.

It must be admitted, however, that there are disadvantages as well. Typical changes in $\bar{D}_z$ are small, on the order of 10%, requiring high precision in measurement. The range of suitable reaction half-lives is rather restricted, between about 200 and 500 s. For slower reactions, complications such as nonspecific aggregate formation or temperature drift can obscure the progress of the reaction. For faster reactions, the quality of the data becomes poorer because shorter accumulation times are required to collect enough data points for the kinetic analysis. Thus, at least for bimolecular reactions, the proper choice of reactant concentrations is crucial to the experiment. Since phage scatter so strongly, very dilute solutions can be used to slow the reaction to a convenient time scale.

References

Aksiyote-Benbasat, J. (1974) Thesis, University of Minnesota, St. Paul, MN.

Aksiyote-Benbasat, J., & Bloomfield, V. A. (1975) *J. Mol. Biol. 95*, 335–357.

Arisaka, F., Tschopp, J., Van Driel, R., & Engel, J. (1979) *J. Mol. Biol. 132*, 369–386.

Bloomfield, V. A., & Lim, T. K. (1978) *Methods Enzymol. 48*, 415–494.

Casjens, S., & King, J. (1975) *Annu. Rev. Biochem. 44*, 555–611.

Coombs, D. H., & Eiserling, F. A. (1977) *J. Mol. Biol. 116*, 375–405.

Cummings, D. J., Kusy, A. R., Chapman, V. A., DeLong, S. S., & Stone, K. R. (1970) *J. Virol. 6*, 534–544.

Debye, P. (1942) *Trans. Electrochem. Soc. 82*, 265.

Geiduschek, E. P., & Holtzer, A. (1958) *Adv. Biol. Med. Phys. 6*, 431–551.

Glasstone, S., Laidler, K. J., & Eyring, H. (1941) in *The Theory of Rate Processes*, McGraw-Hill, New York.

Harrison, D. P., Brown, D. T., & Bode, V. C. (1973) *J. Mol. Biol. 79*, 437–449.

Koppel, D. E. (1972) *J. Chem. Phys. 57*, 4814–4820.

Kunitz, M. (1950) *J. Gen. Physiol. 33*, 363–376.

Moody, M. F. (1965) *Virology 26*, 567–576.

Müller-Salamin, L., Onorato, L., & Showe, M. (1977) *J. Virol. 24*, 121–134.

Pletcher, C. H., Resnick, R. M., Wei, G. J., Bloomfield, V. A., & Nelsestuen, G. L. (1980) *J. Biol. Chem. 255*, 7433–7438.

Smith, R. J., & Cleary, S. F. (1975) *J. Acoust. Soc. Am. 56*, 1883–1889.

Smoluchowski, M. V. (1917) *Z. Phys. Chem., Stoechiom. Verwandtschaftsl. 92*, 129–168.

To, C. M., Kellenberger, E., & Eisenstark, A. (1969) *J. Mol. Biol. 46*, 493–511.

Tschopp, J., Arisaka, F., van Driel, R., & Engel, J. (1979) *J. Mol. Biol. 128*, 247–258.

Tsugita, A., Black, L. W., & Showe, M. K. (1975) *J. Mol. Biol. 98*, 271–275.

Wei, G. J., & Bloomfield, V. A. (1980) *Anal. Biochem. 101*, 245–253.

Wilson, R. W., & Bloomfield, V. A. (1979) *Biopolymers 18*, 1543–1549.

Appendix: Calculation of the Steric Factors Affecting the Head–Tail Joining Reaction

We attempt a quantitative treatment of the steric, electrostatic, and rotational diffusion factors entering the head–tail joining reaction in order to determine the area of the reactive surface patch.

We model the head as a sphere of radius R_H, with the reactive patch occupying a circle described by polar angle θ_H surrounding the "North Pole". The tail, actually a complex structure with the rodlike tube and sheath surmounting the baseplate, is also formally modeled as a sphere with radius R_T and reactive patch angle θ_T at the end away from the baseplate. In both cases, the geometrical radius is assumed equal to the

hydrodynamic radius determined from the diffusion coefficient and Stokes' law.

The area of the reactive patch, assumed equal for heads and tails, is

$$A_P = R_i^2 \int_0^{2\pi} d\phi \int_0^{\theta_i} \sin\theta \, d\theta = 2\pi R_i^2(1 - \cos\theta_i) \quad \text{(A1)}$$

where i = H or T. Thus the reactive fraction of the total surface area of each sphere is

$$F_i = A_P/4\pi R_i^2 = (1 - \cos\theta_i)/2 \quad \text{(A2)}$$

and the probability that the two patches will be opposite each other is

$$F = F_H F_T = (1 - \cos\theta_H)(1 - \cos\theta_T)/4 \quad \text{(A3)}$$

The overall deviation of the observed bimolecular rate constant from the value for k predicted by eq 8 is the product of three factors:

$$k_{obsd} = kf\delta F \quad \text{(A4)}$$

The first of these, the electrostatic factor f, is evaluated by using eq 9–11. At ionic strength 0.08 M, 293 K, and for the charge product $z_1z_2 = -60$, which gives the best fit to the data in Figure 6, we obtain an acceleration of $f = 9.1$. The second factor, the enhancement of the reaction rate due to rotational diffusion of the reactants, was estimated as $\delta = 2$ from Table I of Schmitz & Schurr (1972).

Since under these conditions of ionic strength and temperature, $k_{obsd}/k = {}^1/_{675}$, we find $F = {}^1/_{12\,300}$. With $R_H = 595$ Å and $R_T = 357$ Å and noting that $R_H^2(1 - \cos\theta_H) = R_T^2(1 - \cos\theta_T)$, we find $\theta_H = 8.5°$ and $\theta_T = 14.2°$. These give a reactive patch area A_P of 2.45×10^4 Å^2.

Reference

Schmitz, K. S.,* & Schurr, J. M. (1972) *J. Phys. Chem. 76*, 534–545.

Physical Mechanism for Regulation of Phosphoenolpyruvate-Dependent Glucose Transport Activity in *Escherichia coli*†

G. T. Robillard* and W. N. Konings

ABSTRACT: The activity of the phosphoenolpyruvate-dependent glucose phosphotransferase system (PTS) in *Escherichia coli* is coupled to the oxidation–reduction potential. It is inhibited when the redox potential is increased above −300 mV either via substrate oxidation or via direct addition of oxidizing agents. Depending on the point of addition, dithiothreitol either blocks or reverses these effects. Inhibition occurs at the level of sugar binding to E_{II}. A sulfhydryl group associated with E_{II} activity undergoes reversible oxidation to, presumably, a disulfide, resulting in the conversion of E_{II} from a reduced, high-affinity form to an oxidized, low-affinity form which has a 10^2–10^3 times lower affinity for the sugar. An identical change in affinity occurs as the result of the generation of a $\Delta\bar{\mu}_{H^+}$ during the oxidation of reduced *N*-methylphenazonium methosulfate or nicotinamide adenine dinucleotide. In this case, uncouplers and ionophores reverse the change. A mechanism is proposed in which the electrical potential difference across the membrane regulates the glucose PTS by shifting the midpoint potential of the E_{II}-associated redox transition to more negative values. As a result, E_{II} is converted to the oxidized, low-affinity state in the presence of a $\Delta\bar{\mu}_{H^+}$.

The phosphoenolpyruvate-dependent sugar phosphotransferase system (PTS) of *Escherichia coli* couples the transport of glucose and certain other hexoses to the hydrolysis of phosphoenolpyruvate (PEP)[1] via a series of phosphoryl-group transfer reactions

$$\text{PEP} + \text{HPr} \underset{Mg^{2+}}{\overset{E_I}{\rightleftharpoons}} \text{P-HPr} + \text{Pyr}$$

$$\text{P-HPr} + \text{hexose}_{out} \underset{Mg^{2+}}{\overset{F_{III},\,E_{II}}{\rightleftharpoons}} \text{HPr} + \text{hexose-P}_{in}$$

[for a review, see Postma + Roseman (1976)]. This system has been implicated in the control of transport of non-PTS substrates by a variety of mechanisms. It exerts control either by inhibiting synthesis of enzymes required for the transport and metabolism of non-PTS substrates (catabolite repression) (Magasanik, 1970) or by regulating the activity of already existing transport systems. McGinnis & Paigen (1969) have shown, for instance, that addition of glucose to cells growing on various carbon sources such as glycerol or lactose resulted in inhibition of the utilization of these solutes. Even though the activity of these systems is somehow controlled by the PTS, the activity of the PTS itself can be modulated when transport of some of these same solutes occurs via secondary transport systems. The physical mechanism for the mutual regulation of these various transport activities will be treated in this report.

Early studies (Englesberg et al., 1961; Hoffee & Englesberg, 1962; Hoffee et al., 1964; Hagihira et al., 1963) of αMGlc

† From the Department of Physical Chemistry, University of Groningen, Nijenborgh 16, 9747 AG, Groningen (G.T.R), and the Department of Microbiology, Biological Center, University of Groningen, Kerklaan 30, 9751 NN Haren, The Netherlands (W.N.K.). *Received November 18, 1980.* This research has been supported in part by the Netherlands Foundation for Chemical Research (S.O.N.) with financial aid from the Netherlands Organization for the Advancement of Pure Research (Z.W.O.).

[1] Abbreviations used: αMGlc, methyl α-glucoside; αMG-P, methyl α-glucoside 6-phosphate; Asc, ascorbate; PMS, *N*-methylphenazonium methosulfate; NEM, *N*-ethylmaleimide; DCPIP, 2,6-dichlorophenolindophenol; CCCP, carbonyl cyanide *m*-chlorophenylhydrazone; FCCP, *p*-(trifluoromethoxy)phenylhydrazone; DTT, dithiothreitol; HOQNO, 2-*n*-heptyl-4-hydroxyquinoline *N*-oxide; DTNB, 5,5′-dithiobis(2-nitrobenzoic acid).

0006-2960/81/0420-5025$01.25/0